

## Direct Observation of Interstitial Dislocation Loop Coarsening in $\alpha$ -Iron

S. Moll, T. Jourdan,\* and H. Lefaix-Jeuland

CEA, DEN, Service de Recherches de Métallurgie Physique, F-91191 Gif-sur-Yvette, France

(Received 2 April 2013; published 3 July 2013)

Interstitial loop coarsening by Ostwald ripening can provide insight into single point defects but is very difficult to observe in  $\alpha$ -iron and many other metals where nanoscale vacancy clusters dissociate and annihilate loops. We show that by implanting helium in the samples at a carefully chosen energy, it is possible to observe Ostwald ripening of loops by transmission electron microscopy during *in situ* isochronal annealings. This coarsening of loops results in a sharp increase of the mean loop radius at around 850 K. Using cluster dynamics simulations, we demonstrate that loops evolve due to vacancy emission and that such experiments give a robust estimation of the sum of the formation and migration free energies of vacancies. In particular, our results are in good agreement with self-diffusion experiments and confirm that entropic contributions are large for the vacancy in  $\alpha$ -iron.

DOI: [10.1103/PhysRevLett.111.015503](https://doi.org/10.1103/PhysRevLett.111.015503)

PACS numbers: 61.72.Cc, 61.72.Ff, 61.72.J-, 66.30.Fq

The kinetics of particle coarsening in materials by Ostwald ripening provides valuable information on physical parameters such as the diffusion coefficient of monomers in the matrix [1] and the interfacial energy [2], or equivalently, the stability of particles [3]. Under irradiation, self-defect clusters are created, which can then evolve by Ostwald ripening upon subsequent annealing. This phenomenon has been observed, for example, in silicon with interstitial loops [4], due to the emission and absorption of interstitials. One difficulty with self-defects is that they are nonconservative species; for example, they can be eliminated or created at surfaces of thin foils used for transmission electron microscopy (TEM) observations. This leads to the so-called nonconservative Ostwald ripening process [5], which can be responsible for the shrinkage of all clusters if surfaces act as strong sinks for self-defects [6]. In the case of  $\alpha$ -iron, thermal vacancies are much more easily created than interstitials by the various elements of the microstructure, owing to the high formation energy of interstitials [7,8]. In general, interstitial loop coarsening can therefore occur only by vacancy emission [9]. However, in addition to surfaces, the presence of vacancy clusters in  $\alpha$ -iron after irradiation provides a powerful source of vacancies, which contributes to the annihilation of interstitial loops and explains why no loop coarsening is seen [10]. A way to drastically reduce vacancy emission by vacancy clusters is to introduce helium in the material. As a noble gas, helium does not interact chemically with atoms of the matrix and tends to cluster inside cavities. Vacancy emission then becomes less favorable because it induces a reduction of the volume available for helium atoms and thus an increase of helium pressure [11]. In this Letter, we show that by implanting helium at an appropriate energy, it is possible to observe dislocation loop coarsening by vacancy emission in  $\alpha$ -iron during subsequent isochronal annealings. Using numerical simulations, we highlight the

fact that self-diffusion coefficients and thus activation free energies can be assessed from these experiments.

Polycrystalline Fe 99.95 at.% was used for the present study. Preimplantation characterizations showed a low dislocation density on the order of  $10^8 \text{ cm}^{-2}$  and a microstructure of large grains ( $\sim 100 \mu\text{m}$ ), so the influence of dislocations and grains as sources and sinks for defects can be safely neglected in the following. Samples were implanted with 60-keV  $^4\text{He}$  ions at room temperature with a flux of  $5.5 \times 10^{12} \text{ He cm}^{-2} \text{ s}^{-1}$  up to a fluence of  $10^{16} \text{ cm}^{-2}$ . This high fluence is chosen to create sufficiently large interstitial loops, which can be identified by TEM after implantation. The energy of helium ions should not be too high in order to limit the number of vacancies created per helium ion, so the effect of helium on the stability of vacancy clusters is significant. After implantation, TEM samples were electropolished from rear side up to the electron transparency without damaging the implanted area. Observation of the as-implanted state shows a homogeneous microstructure of small bubbles and dislocation loops. Although loop nature analysis was not performed, following previous results from the literature we can conclude that they are of interstitial type [12].

*In situ* isochronal annealing was performed in the transmission electron microscope with a temperature ramp of 3 K/min. The mean radii of helium bubbles and dislocation loops were measured far from grain boundaries, to avoid their effect on the loop and bubble microstructures (Fig. 1). It is seen that after a low increase up to around 800 K, the loop radius sharply grows. Once dislocation loops are sufficiently large to interact with each other, they coalesce and form a dislocation network (Fig. 2). Over this range of temperature, the bubble mean radius stays nearly constant and then increases significantly at around 950 K.

To highlight the mechanisms occurring in the thin foil during the isochronal annealing, cluster dynamics (CD)

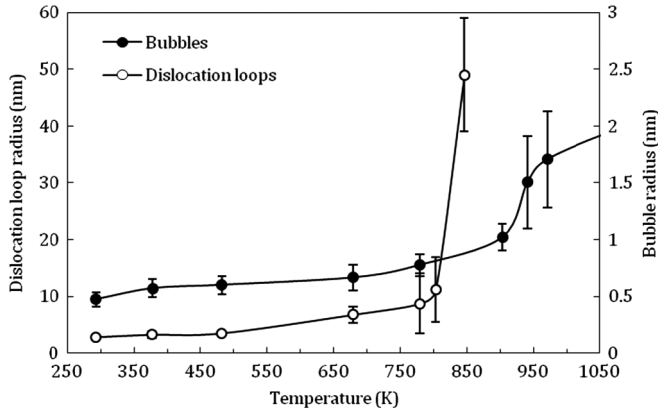


FIG. 1. Evolution of He-bubble and dislocation loop mean radii upon isochronal annealing.

simulations were used. In addition to providing the mean radii of bubbles and loops, such simulations give access to the full helium-vacancy and helium-interstitial cluster distributions so that one can identify the elementary mechanisms that are responsible for the evolution of microstructure. CD simulations consist of solving rate equations whose variables are the concentrations of the different cluster types. Clusters evolve through reactions with other clusters, irradiation, and absorption or emission by sinks (grain boundaries, dislocations). In addition, although CD is based on a mean field formalism, it is possible to consider a one-dimensional dependency of rate equations [13], which proves useful here to simulate the implantation of helium and consider the influence of surfaces.

In our model [14], each cluster type  $\nu$  is identified by its number of vacancies (or interstitials) and helium atoms. We do not detail here the full model but focus instead on the terms that are important for the discussion. For immobile clusters, if the creation rate inside displacement cascades is zero and if the interaction between loops by direct coalescence is ignored, the only evolution comes from emission and absorption of mobile clusters. In this case, the rate equations read

$$\frac{dC_\nu}{dt} = \sum_{\mu \in \mathcal{M}} J_{\nu-\mu,\nu} - \sum_{\mu \in \mathcal{M}} J_{\nu,\nu+\mu}, \quad (1)$$

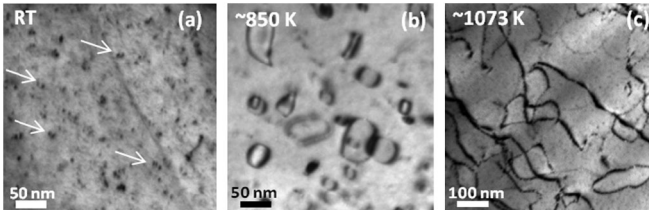


FIG. 2. Dislocation microstructure observed by TEM at (a) 300 K, (b) 850 K, and (c) 1073 K.

where  $\mathcal{M}$  is the set of mobile clusters,  $C_\nu$  is the concentration of cluster class  $\nu$ , and  $J_{\nu,\nu+\mu}$  is a net reactive flux between cluster  $\nu$  and cluster  $\nu + \mu$ , due to the mobility of cluster  $\mu$ . This flux can be written as

$$J_{\nu,\nu+\mu} = \beta_{\nu,\mu} C_\nu C_\mu - \alpha_{\nu+\mu,\mu} C_{\nu+\mu}, \quad (2)$$

where  $\beta_{\nu,\mu}$  and  $\alpha_{\nu+\mu,\mu}$  are absorption and emission rates, respectively. These rates are given by

$$\beta_{\nu,\mu} = 4\pi D_\mu r_{\nu,\mu} \quad (3)$$

and

$$\alpha_{\nu+\mu,\mu} = \frac{\beta_{\nu,\mu}}{V_{\text{at}}} \exp\left(-\frac{F_{\nu+\mu,\mu}^b}{k_B T}\right). \quad (4)$$

In these equations,  $D_\mu$  is the diffusion coefficient of  $\mu$  such that  $D_\mu = D_\mu^0 \exp(-F_\mu^m/k_B T)$ , with  $D_\mu^0$  the diffusion prefactor,  $F_\mu^m$  the migration free energy,  $k_B$  the Boltzmann constant, and  $T$  the temperature. Parameter  $r_{\nu,\mu}$  is an effective interaction distance between clusters  $\nu$  and  $\mu$ ,  $V_{\text{at}}$  is the atomic volume, and  $F_{\nu+\mu,\mu}^b$  is the binding free energy of cluster  $\mu$  to cluster  $\nu$ . Binding energies can be deduced from formation free energies of clusters.

In the parametrization we use here, formation free energies of loops are given by an analytical formula fitted on atomistic calculations using empirical potentials [15]. This approach notably accounts for anisotropic elasticity and contains dislocation core contributions. For bubbles we use also a model fitted on empirical potential calculations, which well reproduces formation energies of bubbles up to high helium-to-vacancy ratios [16]. Formation and migration energies of small clusters are given by density functional theory calculations [17,18]. In high-purity  $\alpha$ -iron, it is well-known theoretically [19,20] and experimentally [21] that interstitial loops are mobile. However, loops were found immobile in our TEM observations, probably due to the presence of impurities and helium, which significantly affect loop mobility [22–25]. Previous CD simulations have already made the assumption of loop trapping by helium atoms [26]. For all these reasons, no loop mobility was considered in the present calculations.

Helium implantation is simulated by CD, using a homogenization procedure of cascades to provide an effective irradiation term accounting for spatial correlations between defects [27]. Cascades are produced by the MARLOWE code [28]. Although using a code based on the binary collision approximation does not reproduce all features of molecular dynamics simulations [29], it proves to be convenient to simulate a large number of cascades and obtain good statistics for the CD irradiation term. In addition, it gives an estimation of spatial correlations that can notably explain the enhanced nucleation rate with respect to homogeneous irradiation by high-energy electrons [12]. Loop and bubble distributions obtained by CD at the end of

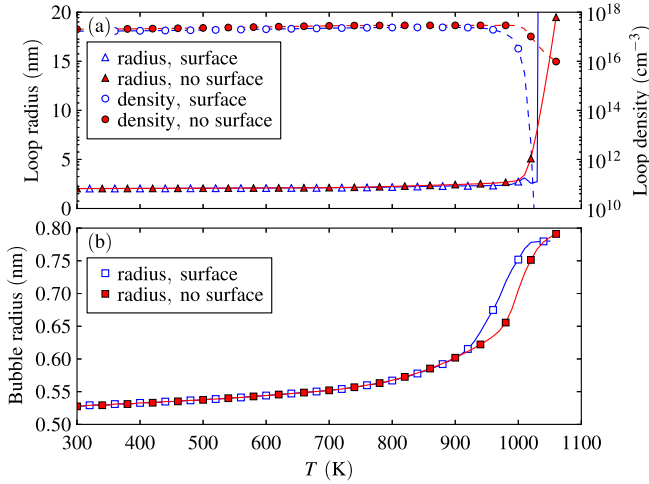


FIG. 3 (color online). Simulated evolution of the loop and bubble microstructures with and without surfaces: (a) loop mean radius and density and (b) bubble mean radius.

the implantation phase are then used as initial distributions for the annealing phase [Supplemental Material [30]].

For the isochronal annealing without irradiation, two cases are considered: in one case a 100 nm-thick thin foil is simulated, whereas in the other case surfaces are not considered. The mean radii of loops and bubbles are shown in Fig. 3 in the two cases. The first thing to note is that the sharp increase of the dislocation loop radius is reproduced. In addition, the bubble radius only slightly evolves. Bubbles are indeed shown to be overpressurized after implantation [Ref. [14] and Supplemental Material [30]], so vacancy emission is very low and bubbles grow mostly by self-interstitial emission.

We first focus on the effect of surfaces. As shown in Fig. 3(b), the increase of bubble size occurs at lower temperature when surfaces are considered. This growth is due to the formation of vacancies at surfaces, which are absorbed by bubbles. When surfaces are not taken into account, the increase of bubble size is still present and occurs when interstitial loops start growing. This simultaneous evolution is consistent with a mechanism involving the emission of vacancies by interstitial loops, followed by their absorption by bubbles and loops. To explain the shift in temperature, we consider the binding energy of a vacancy  $v$  to a loop  $i_{n+1}$  containing  $n + 1$  atoms

$$F_{i_n, v}^b = F_v^f + F_i^f - F_{i_{n+1}, i}^b, \quad (5)$$

where  $F_v^f$  and  $F_i^f$  are the formation free energies of a vacancy and an interstitial, respectively, and  $F_{i_{n+1}, i}^b$  is the binding free energy of an interstitial to an interstitial loop containing  $n$  atoms. As  $F_{i_{n+1}, i}^b$  is lower than  $F_i^f$  and tends towards this value when  $n$  is large,  $F_{i_n, v}^b$  is always larger than  $F_v^f$ . If we assume that the formation free energy of a vacancy at surfaces is the same as in the bulk, the creation

rate of vacancies by surfaces is proportional to  $\exp(-F_v^f/k_B T)$  and is therefore larger than the creation rate of vacancies by loops [Eq. (4)]. This explains why the evolution of bubbles occurs at lower temperature in the presence of surfaces in our simulations.

The role of thermal vacancies emitted by surfaces is not seen in our experiments before loop growth. Instead, a clear increase of the bubble radius is observed at 950 K, which may be ascribed to the emission of vacancies by surfaces. This discrepancy with simulations may be due to the fact that surface contamination cannot be avoided and is possibly responsible for a loss of efficiency of surfaces as vacancy sources. Such variations in sink strength, depending on the surface state, have already been observed in silicon [31]. Another argument in favor of a high temperature emission of vacancies by surfaces is given by the loop evolution in numerical simulations. When surfaces are considered, loop growth is observed, but the absorption of thermal vacancies provided by surfaces is so large that the density of dislocation loops is below the observation limit [Fig. 3(a)]. Such a disappearing of loops is not seen experimentally. In the following we do not consider surfaces, since their effect appears at high temperature in experiments, and we focus on the evolution of the dislocation loops.

As discussed previously, the main mechanism responsible for loop growth is vacancy emission. During this growth, the dislocation loop density decreases. Following Eq. (5), the emission rate of vacancies is greater for large loops than for small loops, so small loops shrink when large loops grow. In other words, the chemical potential of a vacancy in the matrix near a large loop is higher than that close to a small loop. The interstitial loop evolution is therefore affected by an Ostwald ripening process due to vacancy emission.

To assess the interplay between the bubble microstructure and the loop evolution, isochronal annealings were simulated with the same loop microstructure after implantation but without helium and bubbles. In addition, to estimate the influence of helium trapped inside bubbles, another simulation was performed with the bubble microstructure, but helium was removed from bubbles, thus creating voids. As shown in Fig. 4, when bubbles are not taken into account, the loop radius closely follows the evolution obtained when the full microstructure is taken into account. The very stable bubble microstructure only plays a role by emitting self-interstitials, which induces a slight growth of loops. However, if helium is removed from bubbles, the loop evolution is drastically different. Since the binding energy of vacancies to voids  $F_{v, v}^b$  is smaller than the formation energy of a vacancy  $F_v^f$ , dissociation of voids occurs before the emission of vacancies by surfaces and thus by loops is active. This provides a powerful source of vacancies, which annihilate the loops. Therefore, the presence of overpressurized bubbles is necessary to avoid

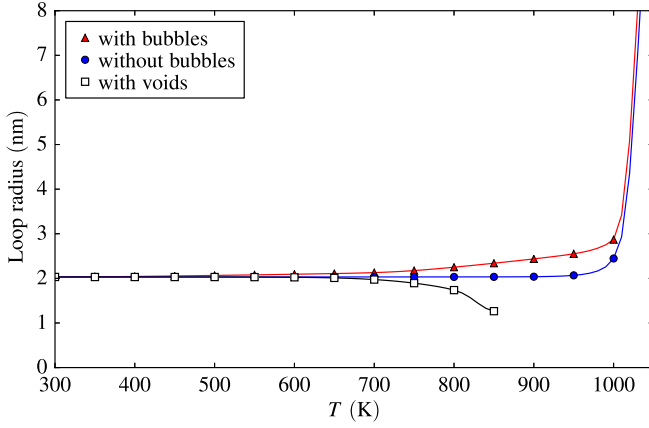


FIG. 4 (color online). Simulated evolution of mean loop radius with various cavity microstructures and no surface.

loop annihilation but does not play any role in loop growth, so we can conclude that we are probing the sole energetic properties of loops during the sharp increase of loop radius.

It is thus tempting to relate the temperature at which the loop radius abruptly increases to some key parameters, in order to improve the model parametrization. Experimentally, the evolution of loops is seen at around 850 K, whereas in numerical simulations it occurs at 1050 K, so the parametrization is not satisfactory. Inspection of Eq. (4), together with Eq. (5) and the expression of the vacancy diffusion coefficient, show that the temperature at which the transition occurs essentially depends on  $D_v^0$  and on the sum of activation free energies  $F_v^f + F_v^m$ . Values that were taken in the previous calculations ( $F_v^f = 2.12$  eV,  $F_v^m = 0.67$  eV) do not include any entropy term and rely on a crude approximation of the diffusion prefactor, using a value close to the Debye frequency as an attempt frequency ( $\nu_0 = 10^{13}$  Hz). Various studies have provided estimates for the formation entropy [32]  $S_v^f$ , the migration entropy [33]  $S_v^m$ , or the sum of both terms [34], but their values remain controversial, especially at high temperature where magnetic contribution is expected to play a role.

However, it can be seen that the vacancy emission rate by loops is proportional to the self-diffusion coefficient in  $\alpha$ -iron  $D_{Fe} = fD_v^0 \exp[-(H_v^f + H_v^m)/k_B T]$ , multiplied by a term which accounts for curvature effects. In this expression  $f$  is the correlation factor ( $f = 0.727$ ). Entropic contributions are only contained in the diffusion prefactor, since enthalpies  $H_v^f$  and  $H_v^m$  are used instead of free energies  $F_v^f$  and  $F_v^m$ . A fit for  $T < 850$  K of self-diffusion coefficient measured experimentally gives [35]  $H_v^f + H_v^m = 2.85$  eV and  $\nu_0 = 5 \times 10^{15}$  Hz. These values, compared to our previous data set, show that the entropic contributions are large and that the self-diffusion coefficient and thus the emission rate by loops were underestimated. Using the Debye frequency as a reference, we find

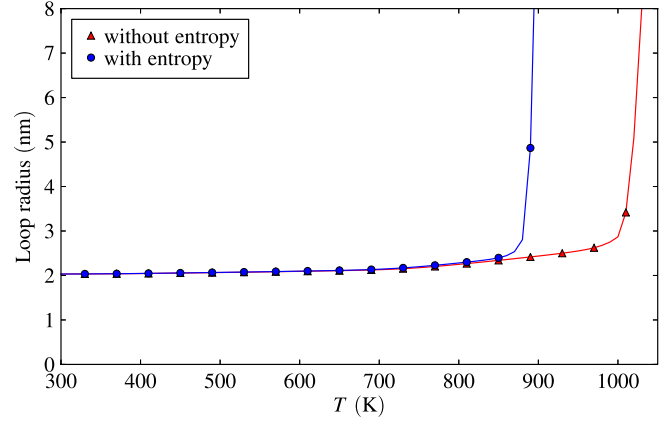


FIG. 5 (color online). Simulated evolution of loop radius with different parameters for the vacancy. Triangles:  $H_v^f + H_v^m = 2.79$  eV,  $\nu_0 = 10^{13}$  Hz; circles:  $H_v^f + H_v^m = 2.85$  eV,  $\nu_0 = 5 \times 10^{15}$  Hz.

$S_v^f + S_v^m = 6.2k_B$ . Although the distinction between the formation and migration terms is arbitrary and does not play any role for our annealings, we choose  $H_v^f = 2.18$  eV,  $H_v^m = 0.67$  eV,  $S_v^f = 4k_B$ , and  $S_v^m = 2.2k_B$ , in good agreement with previous studies [32,33]. Simulations performed with the old and the new data sets are shown in Fig. 5. A much better agreement with experiment is obtained with the new values, which highlights the importance of taking into account entropic contributions at these temperatures. It should be noted that part of the discrepancy between experiments and simulations could also come from the parametrization of loop energetics, which is responsible for the curvature effect mentioned above. Although the onset of loop growth can be affected by this parametrization, for large values of radii dislocation loops are similar to straight dislocations from a thermodynamic point of view. Vacancy emission is governed in this case by the formation and migration free energies of vacancies, so we can conclude that the temperature at which loops grow should not depend significantly on the parametrization of loops. Another source of discrepancy between simulations and experiments could come from the release of helium from bubbles, which cannot be probed by our TEM observations and which could affect the loop growth. We performed thermal helium desorption experiments on the same type of samples with the same implantation conditions [Supplemental Material [30]] and found that the quantity of helium released is very low over the temperature range investigated here, in agreement with our calculations. Therefore, helium release probably does not significantly influence the temperature at which loops evolve.

To conclude, loop coarsening by vacancy emission was observed in  $\alpha$ -iron during isochronal annealings, which leads to a sharp variation of loop radius at around 850 K. This phenomenon is seen because other sources of

vacancies that would annihilate loops are not sufficiently efficient. In particular, due to helium implantation, vacancy clusters are overpressurized and cannot significantly emit vacancies. The temperature at which loops quickly grow can be closely connected to the sum of the formation and migration free energies of the vacancy. A good agreement has been obtained with activation energies deduced from self-diffusion experiments. The methodology described in the present work is expected to be transferable to other metals for which the formation energy of vacancies is much lower than the formation energy of interstitials.

This work was partially funded by the French National Research Agency (ANR) through the HSynThEx project ANR-10-INTB-0905. The authors thank A. Barbu, M.-C. Marinica, and F. Soisson for valuable discussions.

---

\*thomas.jourdan@cea.fr

- [1] A. J. Ardell, in *Phase Transformations '87*, edited by G. W. Lorimer (Institute of Metals, London, 1988), p. 485.
- [2] A. J. Ardell, *Metall. Trans.* **1**, 525 (1970).
- [3] N. E. B. Cowern, G. Mannino, P. A. Stolk, F. Roozeboom, H. G. A. Huizing, J. G. M. van Berkum, F. Cristiano, A. Claverie, and M. Jaraíz, *Phys. Rev. Lett.* **82**, 4460 (1999).
- [4] C. Bonafos, D. Mathiot, and A. Claverie, *J. Appl. Phys.* **83**, 3008 (1998).
- [5] Y. L. Huang, M. Seibt, and B. Plikat, *Appl. Phys. Lett.* **73**, 2956 (1998).
- [6] H. G. Bowden and R. W. Balluffi, *Philos. Mag.* **19**, 1001 (1969).
- [7] C. Domain and C. S. Becquart, *Phys. Rev. B* **65**, 024103 (2001).
- [8] C. C. Fu, F. Willaime, and P. Ordejón, *Phys. Rev. Lett.* **92**, 175503 (2004).
- [9] B. Burton and M. V. Speight, *Philos. Mag. A* **53**, 385 (1986).
- [10] K. Ono, K. Arakawa, H. Shibasaki, H. Kurata, I. Nakamichi, and N. Yoshida, *J. Nucl. Mater.* **329–333**, 933 (2004).
- [11] C. C. Fu and F. Willaime, *Phys. Rev. B* **72**, 064117 (2005).
- [12] K. Arakawa, R. Imamura, K. Ohta, and K. Ono, *J. Appl. Phys.* **89**, 4752 (2001).
- [13] D. Xu, X. Hu, and B. D. Wirth, *Appl. Phys. Lett.* **102**, 011904 (2013).
- [14] T. Jourdan, G. Bencteux, and G. Adjanor (to be published).
- [15] S. L. Dudarev, R. Bullough, and P. M. Derlet, *Phys. Rev. Lett.* **100**, 135503 (2008).
- [16] T. Jourdan and J.-P. Crocombette, *J. Nucl. Mater.* **418**, 98 (2011).
- [17] C.-C. Fu, J. Dalla Torre, F. Willaime, J.-L. Bocquet, and A. Barbu, *Nat. Mater.* **4**, 68 (2005).
- [18] C. C. Fu and F. Willaime, *J. Nucl. Mater.* **367–370**, 244 (2007).
- [19] B. D. Wirth, G. R. Odette, D. Maroudas, and G. E. Lucas, *J. Nucl. Mater.* **276**, 33 (2000).
- [20] N. Soneda and T. Diaz de la Rubia, *Philos. Mag. A* **81**, 331 (2001).
- [21] K. Arakawa, K. Ono, M. Isshiki, K. Mimura, M. Uchikoshi, and H. Mori, *Science* **318**, 956 (2007).
- [22] J. Marian, B. D. Wirth, A. Caro, B. Sadigh, G. R. Odette, J. M. Perlado, and T. Diaz de la Rubia, *Phys. Rev. B* **65**, 144102 (2002).
- [23] K. Tapasa, A. V. Barashev, D. J. Bacon, and Y. N. Osetsky, *J. Nucl. Mater.* **361**, 52 (2007).
- [24] Y. Satoh, H. Matsui, and T. Hamaoka, *Phys. Rev. B* **77**, 094135 (2008).
- [25] L. Ventelon, B. Wirth, and C. Domain, *J. Nucl. Mater.* **351**, 119 (2006).
- [26] J. Marian and V. V. Bulatov, *J. Nucl. Mater.* **415**, 84 (2011).
- [27] T. Jourdan and J.-P. Crocombette, *Phys. Rev. B* **86**, 054113 (2012).
- [28] M. T. Robinson, *Phys. Rev. B* **40**, 10717 (1989).
- [29] P. Erhart and J. Marian, *J. Nucl. Mater.* **414**, 426 (2011).
- [30] See Supplemental Material at <http://link.aps.org/supplemental/10.1103/PhysRevLett.111.015503> for the cluster distribution obtained by simulation at the end of the implantation phase and for thermal helium desorption and differential scanning calorimetry experiments.
- [31] F. Cristiano, J. Grisolia, B. Colombeau, M. Omri, B. de Mauduit, A. Claverie, L. F. Giles, and N. E. B. Cowern, *J. Appl. Phys.* **87**, 8420 (2000).
- [32] G. Lucas and R. Schäublin, *Nucl. Instrum. Methods Phys. Res., Sect. B* **267**, 3009 (2009).
- [33] M. Athènes and M.-C. Marinica, *J. Comput. Phys.* **229**, 7129 (2010).
- [34] A. Seeger, *Phys. Status Solidi (A)* **167**, 289 (1998).
- [35] F. Soisson and C.-C. Fu, *Phys. Rev. B* **76**, 214102 (2007).